Effect of Controlled Growth Dynamics on the Microstructure of Nonpolar *a*-Plane GaN Revealed by X-ray Diffraction

2009 Jpn. J. Appl. Phys. 48 071002

(http://iopscience.iop.org/1347-4065/48/7R/071002)

Effect of Controlled Growth Dynamics on the Microstructure of Nonpolar *a*-Plane GaN Revealed by X-ray Diffraction

Qian Sun[1], Tsung-Shine Ko[1,2], Christopher D. Yerino[1], Yu Zhang[1], In-Hwan Lee[1*], Jung Han[1†], Tien-Chang Lu[2], Hao-Chung Kuo[2], and Shing-Chung Wang[2]

[1]*Department of Electrical Engineering, Yale University, New Haven, CT 06520, U.S.A.*
[2]*Department of Photonics and Institute of Electro-Optical Engineering, National Chiao Tung University, 1001 Ta Hsueh Rd., Hsinchu 30050, Taiwan*

Received January 8, 2009; accepted April 22, 2009; published online July 21, 2009

This paper reports the effect of controlled growth dynamics, as monitored by *in situ* optical reflectance, on the microstructure of nonpolar *a*-plane GaN films grown on *r*-plane sapphire. The mosaic microstructure of *a*-plane GaN and its anisotropy are evaluated by X-ray rocking curve (XRC) measurements. By inserting a pronounced islanding stage followed by an enhanced lateral growth, pit-free *a*-plane GaN has been achieved showing an XRC linewidth of ~0.18 and ~0.3° for on- and off-axes planes, respectively, with only minor anisotropy. The density of basal-plane stacking faults is reduced by ~70% as determined by a modified Williamson–Hall X-ray analysis.

DOI: 10.1143/JJAP.48.071002

1. Introduction

In the heteroepitaxy of nonpolar *a*-plane GaN (*a*-GaN), two major issues are the poor surface morphology with triangular/pentagonal surface pits[1–3] and the presence of a high density of structural defects, including threading dislocations (TDs) and basal-plane stacking faults (BSFs) bounded by partial dislocations (PDs).[4–8] In the study of *c*-plane GaN (*c*-GaN) growth, an intentional three-dimensional (3D) to two-dimensional (2D) transition (a roughening-recovery process) was found crucial in achieving improved crystalline quality.[9–12] Applying this concept, Hollander *et al.*[3] reported that a two-step *a*-GaN growth procedure (beyond the initial buffer layer) with different V/III ratios can empirically reduce the linewidth of the on-axis X-ray rocking curve (XRC). To establish a basis for interpreting the complex morphology in nonpolar GaN heteroepitaxy, we recently employed selective area growth (SAG) to map out kinetic Wulff plots (*v*-plots) for polar, semipolar, and nonpolar orientations.[2] The knowledge of *v*-plots enables in the present study a rational control of the growth dynamics for *a*-GaN on *r*-plane sapphire (*r*-sapphire). The degree of the initial roughening can be tailored by controlling the vertical versus lateral growth rates. Rapid island coalescence leading to a pit-free morphology was attained using conditions that facilitate lateral growths. A significant improvement in the microstructural quality of the *a*-GaN films is correlated with the insertion of a 3D-growth stage. The nature and anisotropy of defects were examined by XRC using on- and *off-axes* diffraction planes spanning over a broad steradian angular range.

2. Experiment

All the *a*-GaN samples were grown on nominally on-axis *r*-sapphire (substrate nitridation is adopted[13]) in a horizontal metalorganic chemical vapor deposition reactor. A 60-nm-thick AlN buffer was grown at 1150 °C. For the baseline (sample A), 2-μm-thick *a*-GaN was directly grown on the AlN buffer at 1050 °C, a reactor pressure, *P*, of 60 mbar and a V/III ratio of 187. For all other samples (B–F) a 3D-growth stage was introduced with various *P* and V/III (Table I) to control the growth dynamics, before returning to the baseline condition. Sample F, having the longest roughening growth stage, was grown nominally twice as thick as other samples to ensure a fully coalesced surface. The sample surfaces were examined by scanning electron microscope (SEM; FEI XL30 field-emission microscope). A normal-incidence optical reflectometer (wavelength = 900 nm) was implemented to monitor all the *a*-GaN growths. The *in situ* optical reflectance is a powerful real-time tool and has been widely utilized for studying the surface roughness, layer thickness, and the growth evolution dynamics.[9–12] A high resolution X-ray diffractometer (Bede D1) was employed to examine the effect of the controlled growth dynamics on the microstructure of the *a*-GaN films. Double-crystal XRCs were measured in symmetric and skew symmetric geometry for on-axis and off-axis planes, respectively.

Table I. Growth parameters and characterization results of samples A–F.

Sample	1st-step *a*-GaN			*c*-axis LCL (nm)	BSF density $\times 10^5$ cm^{-1}
	V/III	P (mbar)	t (min)		
A	—	—	0	19	5.3
B	1440	60	10	24.5	4.1
C	2162	100	17	30.4	3.3
D	2162	200	17	36.5	2.7
E	1682	300	17	45.4	2.2
F	1682	300	40	60	1.7

3. Results and Discussion

For sample A (one step growth), the *in situ* reflectance trace exhibits instant oscillations [Fig. 1(a)] indicating a quasi-2D growth mode. This observation agrees well with the *v*-plots[2] that the growth condition for sample A suppresses the vertical *a*-axis growth and promotes lateral growths. Our earlier study[2] of *v*-plots further indicated that the vertical growth can be greatly enhanced while the lateral growth (especially along the *c*-axis) is slowed down under an increased V/III ratio and/or an elevated *P*, thus facilitating the formation of *a*-GaN islands with a "tall" aspect ratio. Such knowledge was incorporated into the design of a "two-step" procedure to induce a 3D islanding stage and to test

*On sabbatical leave from School of Advanced Materials Engineering, Chonbuk National University, Jeonju 561-756, Korea.
†E-mail address: jung.han@yale.edu

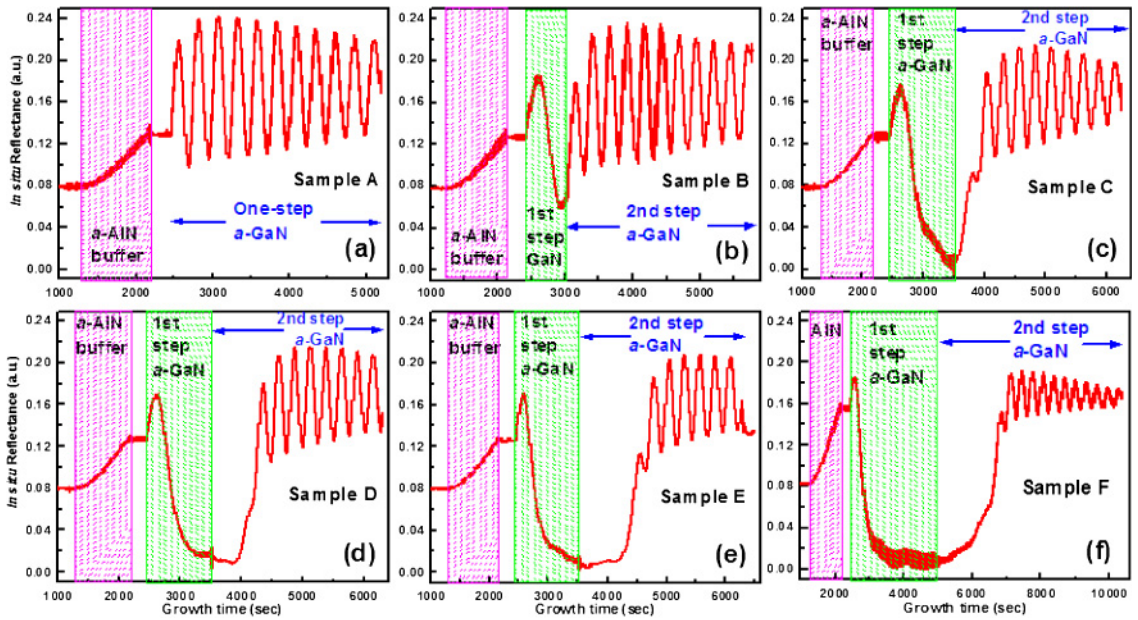

Fig. 1. (Color online) *In situ* optical reflectance traces of *a*-GaN growths for samples A (a), B (b), C (c), D (d), E (e), and F (f). The reflectance segments shaded in green in (b)–(f) correspond to the 1st-step 3D *a*-GaN growth for samples B–F.

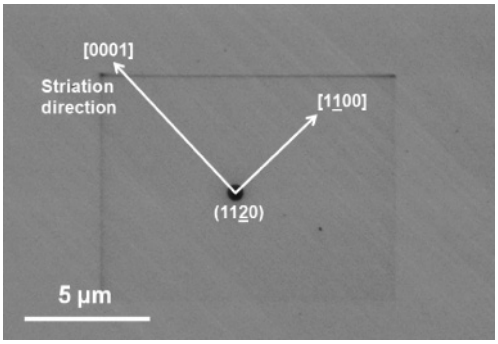

Fig. 2. SEM image of the *a*-GaN surface of sample F, showing no surface pits. The black square shadow is due to the charging of electron beam during the SEM image focusing.

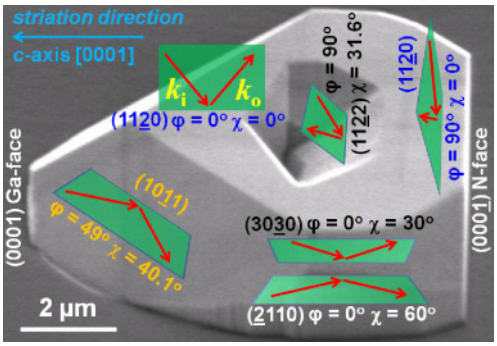

Fig. 3. (Color online) SEM image of an *a*-GaN SAG mesa with both convex and concave growth fronts (grown out of an annular ring opening) for the illustration of XRC configurations. For $\varphi = 0$ and 90°, the X-ray rocking direction is parallel and perpendicular to the *c*-axis [0001], respectively. The incident and diffracted X-ray beams (red arrows) rock within a plane (shaded in green) for each diffraction plane with its index and orientation labeled in the vicinity. The on-axis (11$\underline{2}$0) ($\chi = 0°$) and off-axis planes ($\chi \neq 0°$), such as (10$\underline{1}$1), (2$\underline{1}$10), (30$\underline{3}$0), and (11$\underline{2}$2), were measured in symmetric and skew symmetric geometries, respectively.

both the controllability and effect. During the 1st-step growth of samples B–F, as the V/III ratio and/or P increase, surface becomes increasingly rough as revealed by the progressive decay of the reflectance traces,[14] eventually down to nearly background [Figs. 1(b)–1(f)]. Once the growth is switched back to the baseline condition (for the second-step growth), island coalescence through lateral growth occurs at a rate that is inversely correlated with the extent of roughening after the 1st-step growth. The amplitude of reflectance oscillations decreases from sample A to F because of their increased surface roughening, but the average of reflectance oscillations remains similar. All the samples exhibit a pit-free surface under SEM, as shown in Fig. 2 for sample F.

In *a*-GaN films, TDs have different characteristics from those in *c*-GaN. Pure screw TDs have Burgers vectors $\mathbf{b}_s = \pm 1/3[11\underline{2}0]$, and pure edge TDs $\mathbf{b}_e = \pm[0001]$. Due to the reduced symmetry of *a*-GaN surface, there are three kinds of mixed type TDs, (1) $\mathbf{b}_{m1} = \pm 1/3[1\underline{2}10]$ or $\pm 1/3[\underline{2}110]$, (2) $\mathbf{b}_{m2} = \pm 1/3[11\underline{2} \pm 3]$, and (3) $\mathbf{b}_{m3} = \pm 1/3[1\underline{2}1 \pm 3]$ or $\pm 1/3[\underline{2}11 \pm 3]$.[4] It has been commonly observed that the BSFs in *a*-GaN are mostly of I_1 type, normally bounded by Frank–Shockley PDs with $\mathbf{b}_p = \pm 1/6[20\underline{2} \pm 3]$, $\pm 1/6[02\underline{2} \pm 3]$, or $\pm 1/6[2\underline{2}0 \pm 3]$.[5–8] Given the complexity of TDs/PDs, it is necessary to measure XRCs for both on- and *off-axes* planes over a sufficiently large azimuthal and polar angular space (Fig. 3) to obtain a comprehensive knowledge of the microstructure of *a*-GaN. The full widths at half maximum (FWHMs) were obtained through fitting with pseudo-Voigt functions.[15]

Figure 4(a) shows the FWHM of the on-axis (11$\underline{2}$0) XRCs as a function of the azimuthal angle, φ. The φ angle is set at 0 and 90° when the rocking direction of the incident and diffracted X-ray beams is parallel and perpendicular to the *c*-axis [0001] (the striation direction), respectively (Fig. 3). The baseline sample A (with instant reflectance oscillations) exhibits very anisotropic FWHMs for the on-axis (11$\underline{2}$0) XRCs, similar to many previous reports.[1,3,16,17] However, with the introduction of a 3D growth stage, the FWHM of

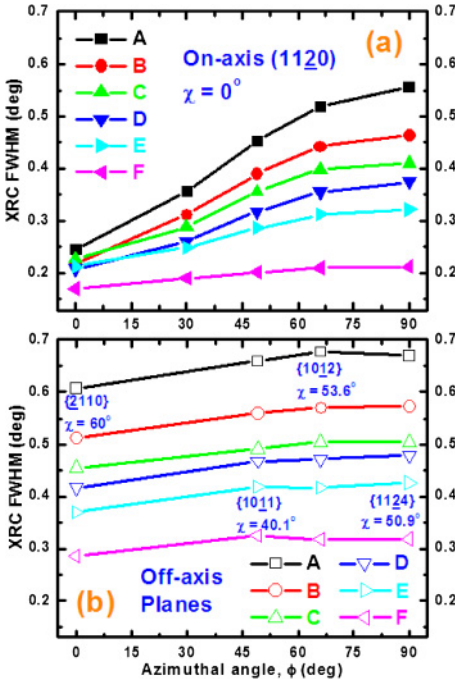

Fig. 4. (Color online) The FWHM of the on-axis (a) and off-axis (b) XRCs of *a*-GaN as a function of the azimuthal angle, φ.

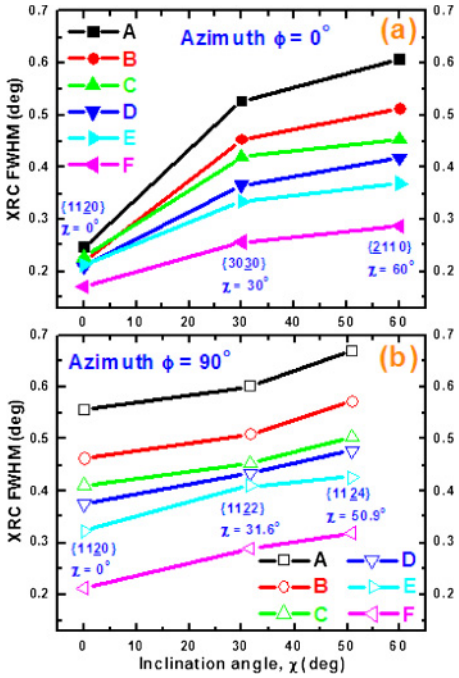

Fig. 5. (Color online) The FWHM of *a*-GaN XRCs as a function of the plane inclination angle, χ, for two sets of planes at $\varphi = 0$ (a) and 90° (b).

the on-axis (11$\underline{2}$0) XRC at $\varphi = 90°$ decreases monotonically from sample A to F, and the FWHM-φ plots become less steep, indicative of improved isotropy. Given the insensitivity of (11$\underline{2}$0) diffraction to BSFs,[8,18] the anisotropic broadening of the on-axis (11$\underline{2}$0) XRCs is due to the anisotropy in mosaic tilt and/or domain size (the influence of BSFs is not considered here).[15,19] The former is related to the angular distribution of TDs/PDs with a screw component; and the latter may be induced by the asymmetry in lattice mismatch between *a*-GaN and *r*-sapphire along the two orthogonal in-plane axes. The high mismatch along the *m*-axis (~16%) and the much smaller mismatch along the *c*-axis (~1.2%) may energetically favor the formation of highly elongated *a*-GaN nuclei along the *c*-axis, causing anisotropic broadening in the on-axis (11$\underline{2}$0) XRCs. According to the *v*-plots,[2] however, the 1st-step growth conditions (high V/III ratio and high P) may kinetically help produce *a*-GaN nucleation islands in a more isotropic shape. A Williamson–Hall (WH) X-ray study[15,19,20] of the on-axis *a*-plane at $\varphi = 0$ and 90° is now underway to decouple the contributions of mosaic tilt and domain size to the on-axis XRC broadening.

Mosaic twist (in-plane misalignment) is an important aspect of the microstructure and normally correlated with TDs/PDs with an edge component,[15,19] a subject that has been studied only briefly for *a*-GaN film.[4,17] To study twist in the *a*-GaN films, XRC measurements were implemented in a *skew* symmetric geometry for *off-axis* planes having an inclination angle χ with respect to the on-axis (11$\underline{2}$0) at various azimuths (Fig. 3). The planes involved in this study are ($\underline{2}$110), (10$\underline{1}$1), (10$\underline{1}$2), (11$\underline{2}$2), and (11$\underline{2}$4) with a (φ, χ) setting of approximately (0°, 60°), (49°, 40°), (66°, 54°), (90°, 32°), and (90°, 51°), respectively. The (φ, χ) angles of the off-axis planes were determined with the aid of *a*-GaN SAG mesa (with both *convex* and *concave* growth fronts) grown out of an annular ring opening (Fig. 3).[2] As shown in Fig. 4(b), for all the samples the FWHM–φ plots of the off-axis XRCs are fairly flat with a small anisotropy [unlike the case of on-axis XRCs in Fig. 4(a)], implying a uniform angular distribution of TDs/PDs with an edge component. For sample A (with no intentional 3D growth), the off-axis XRC FWHMs are very high, ranging from 0.6 to 0.7°. With the insertion of 3D island growths, the off-axis XRC FWHMs decrease *evenly* for all the azimuths from samples B to F, reaching a ~50% reduction for the case with a prolonged 3D growth. The off-axis XRC FWHM (~0.3°) of sample F (~4 μm thick) is among the lowest reported so far for *a*-GaN grown on *r*-sapphire.

To obtain a more detailed picture of the mosaic tilt/twist distribution in *a*-GaN, we further studied χ-plots at two orthogonal azimuths (Fig. 5). The χ-plot is an established procedure to extract the in-plane misalignment for *c*-GaN.[19,21] The both χ-plots in Fig. 5 show that, for all the samples, the FWHMs increase as χ increases, indicating that there is more twist than tilt. It has been reported that the majority of dislocations in *a*-GaN are I_1-BSF-related Frank–Shockley PDs with $\mathbf{b}_p = 1/6\langle 2\underline{2}03\rangle$.[7] And the *uniform* reduction in twist for all the azimuths [Fig. 4(b)] implies that the twist at various azimuths may be attributed to the same origin. Hence we speculate that it is the in-plane components ($\mathbf{b} = 1/2\langle 0001\rangle$ and $\mathbf{b} = 1/3\langle 1\underline{1}00\rangle$ from $\mathbf{b}_p = 1/6\langle 2\underline{2}03\rangle$)[8] of I_1-BSF-related Frank–Shockley PDs that mainly account for the twist as χ approaches 90° towards the in-plane *c*- and *m*-axes, respectively. From sample A to F, the monotonic reduction (> 50%) in FWHM for both the on- and off-axes XRCs (Figs. 4 and 5) is clear evidence that the crystalline quality of the *a*-GaN films is substantially improved through the inserted 3D-and-2D growth process. As shown in Fig. 3, *a*-GaN islands normally have *inclined* sidewalls, such as (10$\underline{1}$1) and (10$\underline{1}$0).[2] During the 3D island growth and/or the subsequent island coalescence, the TDs/PDs within the

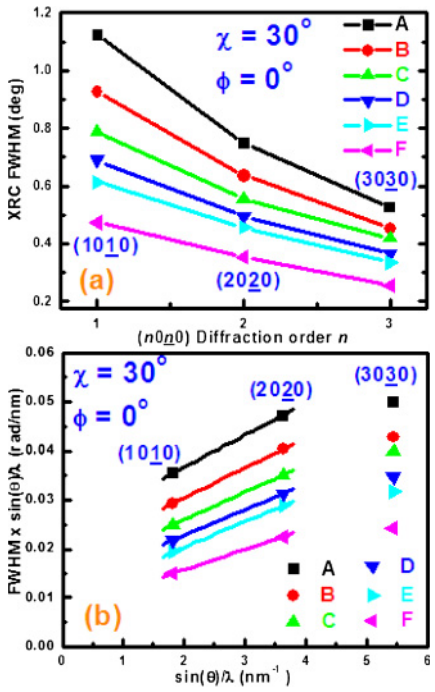

Fig. 6. (Color online) (a) The FWHMs of *m*-plane ($n0\underline{n}0$) XRCs ($n = 1$, 2, and 3; $\varphi = 0°$, $\chi = 30°$); (b) the modified WH plots. The straight lines in (b) are the linear fits to the ($10\underline{1}0$) and ($20\underline{2}0$) data-points of each sample.

islands may bend at the inclined growth fronts,[22,23] and annihilate via their interaction with each other.

Recently, McLaurin *et al.*[18] proposed a model treating BSFs as boundaries between incoherently scattering domains, and determined the lateral coherence length (LCL) along the *c*-axis in *m*-plane GaN film through a modified WH analysis. The same concept is applied here to determine the *c*-axis LCL and estimate the BSF density in the *a*-GaN films. Because *a*-plane diffraction is insensitive to the presence of BSFs, a modified WH analysis was carried out with *m*-plane ($n0\underline{n}0$) diffraction ($n = 1$, 2, and 3; $\varphi = 0°$, $\chi = 30°$) in a skew symmetric geometry with the X-ray rocking along the *c*-axis (Fig. 3). The XRC FWHMs for all three diffractions decrease monotonically from sample A to F [Fig. 6(a)], another indicator of the clear trend of improved structural quality. It is noted that for all the samples, the FWHMs of ($10\underline{1}0$) and ($20\underline{2}0$) XRCs are much broader than that of ($30\underline{3}0$) XRC, because the former two XRCs are predominantly broadened by the short *c*-axis LCLs due to the presence of BSFs, which is more clearly revealed by the WH plots in Fig. 6(b). Since ($30\underline{3}0$) diffraction is insensitive to the presence of BSFs, the ($30\underline{3}0$) data-points in the WH plots [Fig. 6(b)] are significantly lower than the expected values from the linear fits to the corresponding ($10\underline{1}0$) and ($20\underline{2}0$) data-points of each sample.[18] The *c*-axis LCLs can be derived from the *y*-axis intercepts (y_0) of the linear fits, $\mathrm{LCL} = 0.9/(2y_0)$.[15] And the reciprocal of the LCLs gives the density of BSFs. The determined LCL and BSF density of all the samples are summarized in Table I. It is clearly shown that the more the 3D process is involved in the first-step growth, the longer the *c*-axis LCL and the lower the BSF density. The substantial reduction (~70%) in BSF density is likely related to the bending of PDs and/or the possibly improved GaN nucleation under the first-step growth condition, since zinc-blende nucleation is less favorable under a high V/III condition.[24]

4. Conclusions

In conclusions, a rational design of two-step growth process has been carried out to greatly improve the structural quality of *a*-GaN films. Compared to the very broad XRC FWHMs of the one-step grown *a*-GaN, a substantial reduction (>50%) in XRC FWHM and an increase in *c*-axis LCL (3 times) have been achieved through the roughening-recovery process. A detailed study on the *a*-GaN microstructural evolution is currently in progress to unveil the mechanisms for the reduction of TDs/PDs and BSFs.

Acknowledgement

This work was supported by the US Department of Energy under contract DE-FC26-07NT43227.

1) X. Ni, Y. Fu, Y. T. Moon, N. Biyikli, and H. Morkoç: J. Cryst. Growth **290** (2006) 166.
2) Q. Sun, C. D. Yerino, T. S. Ko, Y. S. Cho, I.-H. Lee, J. Han, and M. E. Coltrin: J. Appl. Phys. **104** (2008) 093523.
3) J. L. Hollander, M. J. Kappers, C. McAleese, and C. J. Humphreys: Appl. Phys. Lett. **92** (2008) 101104.
4) M. D. Craven, S. H. Lim, F. Wu, J. S. Speck, and S. P. DenBaars: Appl. Phys. Lett. **81** (2002) 469.
5) D. N. Zakharov, Z. Liliental-Weber, B. Wagner, Z. J. Reitmeier, E. A. Preble, and R. F. Davis: Phys. Rev. B **71** (2005) 235334.
6) R. Liu, A. Bell, F. A. Ponce, C. Q. Chen, J. W. Yang, and M. A. Khan: Appl. Phys. Lett. **86** (2005) 021908.
7) T. Gühne, Z. Bougrioua, P. Vennéguès, M. Leroux, and M. Albrecht: J. Appl. Phys. **101** (2007) 113101.
8) Z. H. Wu, A. M. Fischer, F. A. Ponce, B. Bastek, J. Christen, T. Wernicke, M. Weyers, and M. Kneissl: Appl. Phys. Lett. **92** (2008) 171904.
9) J. Han, T. B. Ng, R. M. Biefeld, M. H. Crawford, and D. M. Follstaedt: Appl. Phys. Lett. **71** (1997) 3114.
10) S. Figge, T. Bottcher, S. Einfeldt, and D. Hommel: J. Cryst. Growth **221** (2000) 262.
11) D. D. Koleske, A. J. Fischer, A. A. Allerman, C. C. Mitchell, K. C. Cross, S. R. Kurtz, J. J. Figiel, K. W. Fullmer, and W. G. Breiland: Appl. Phys. Lett. **81** (2002) 1940.
12) S. Kim, J. Oh, J. Kang, D. Kim, J. Won, J. W. Kim, and H. K. Cho: J. Cryst. Growth **262** (2004) 7.
13) Q. Sun, Y. S. Cho, I.-H. Lee, J. Han, B. H. Kong, and H. K. Cho: Appl. Phys. Lett. **93** (2008) 131912.
14) R. Miyagawa, M. Narukawa, B. Ma, H. Miyake, and K. Hiramatsu: J. Cryst. Growth **310** (2008) 4979.
15) T. Metzger, R. Höpler, E. Born, O. Ambacher, M. Stutzmann, R. Stömmer, M. Schuster, H. Göbel, S. Christiansen, M. Albrecht, and H. P. Strunk: Philos. Mag. A **77** (1998) 1013.
16) H. Wang, C. Chen, Z. Gong, J. Zhang, M. Gaevski, M. Su, J. Yang, and M. Asif Khan: Appl. Phys. Lett. **84** (2004) 499.
17) A. Chakraborty, K. C. Kim, F. Wu, J. S. Speck, S. P. DenBaars, and U. K. Mishra: Appl. Phys. Lett. **89** (2006) 041903.
18) M. B. McLaurin, A. Hirai, E. Young, F. Wu, and J. S. Speck: Jpn. J. Appl. Phys. **47** (2008) 5429.
19) R. Chierchia, T. Böttcher, H. Heinke, S. Einfeldt, S. Figge, and D. Hommel: J. Appl. Phys. **93** (2003) 8918.
20) G. K. Williamson and W. H. Hall: Acta Metall. **1** (1953) 22.
21) V. Srikant, J. S. Speck, and D. R. Clarke: J. Appl. Phys. **82** (1997) 4286.
22) M. Imura, A. Honshio, K. Nakano, M. Tsuda, M. Iwaya, S. Kamiyama, H. Amano, and I. Akasaki: Jpn. J. Appl. Phys. **44** (2005) 7418.
23) M. D. Craven, S. H. Lim, F. Wu, J. S. Speck, and S. P. DenBaars: Appl. Phys. Lett. **81** (2002) 1201.
24) B. M. Shi, M. H. Xie, H. S. Wu, N. Wang, and S. Y. Tong: Appl. Phys. Lett. **89** (2006) 151921.